Review Paper

Investigation of radionuclide levels and estimation for real emanated radon in rock samples collected from Sinai-Egypt

A. Saber[1] · Hanan. A. S. Aly[2]

Received: 23 July 2022 / Accepted: 12 January 2023
Published online: 27 January 2023
© The Author(s) 2023 OPEN

Abstract
In this work, the distributions of radionuclides activity as well as radon concentrations in selected rock samples collected from Sinai-Egypt were investigated. Radionuclides distribution, ^{238}U, ^{232}Th and ^{40}K, in rock samples, which were gathered from Um-Bogma region, was calculated by HPGe detector. Also radon concentration has been measured by using (SSNTD) CR-39. Using empirical equations, the concentration of ^{222}Rn emitted (^{226}Ra decaying) was computed and compared to the tracks recorded by CR-39. From our data, the average specific activity in Bq kg^{-1} for ^{238}U, ^{235}U, ^{234}U, ^{226}Ra ^{232}Th and ^{40}K were obtained. Measured radon concentrations as generated alpha tracks owing to ^{222}Rn$_m$ (measured radon) were compared to occurring ^{222}Rn$_p$ (predicted radon) as ^{226}Ra alpha decay to determine measured radon loss in natural samples taken from Sinai, Egypt. The geological structure appears to be the main factor affect on detected radon concentration and results shows that radon emanation was influenced by the rock type.

Article highlights

- Radon concentrations from CR-39 recorded tracks were calculated and compared with expected radon emission.
- The difference between the recorded and predicted emanated radon is described by the sample density.

Keywords Radionuclides · HPGe · SSNTD CR-39 · Predicted radon · Emanation coefficient

1 Introduction

For assessing the effects of radiation exposure from terrestrial sources, the distribution of natural radionuclide and radiation level in the environment are of great importance. The Earth contains naturally occurring radioactive materials (NORM). The majority of radionuclides in NORM are radioisotopes including ^{238}U, ^{235}U, ^{226}Ra, ^{232}Th and ^{40}K [1]. Since radionuclides in soil and rock are not evenly dispersed, natural radioactivity is mostly determined by rock formalizations and geographic conditions, resulting in varying quantities of radionuclides in these media. [2, 3]. Large amounts of NORM are produced as a result of mining and other industrial activities [4].

Natural radionuclides may have an effect. Natural background radiation, which is expected to rise to dangerous levels as a result, is a major source of concern to radiation protection regulatory bodies. ^{222}Rn is a daughter of ^{226}Ra and is in turn derived from the longer-lived preceding ^{238}U. Inhalation of radon (^{222}Rn) may cause lung effect [5, 6].

✉ Hanan. A. S. Aly, abdelnaser.soliman@feng.bu.edu.eg | [1]Basic Science Department, Faculty of Engineering at Shoubra, Benha University, Cairo, Egypt. [2]Physics Department, Faculty of Women for Arts, Science and Education, Ain Shams University, Cairo, Egypt.

The Um Bogma Formation in Egypt's south western Sinai is a significant region because it is rich in minerals such as uranium which hosted by manganese and iron Mn-Fe ore deposits as well as copper mineralization [7].

Radon is transmitted by diffusion, transportation mechanisms, or a combination of the two [8]. The favoured mechanism is affected by geological structure, porosity, and permeability of rocks and soils, as well as ground water flow and meteorological conditions [9]. Sedimentary Rocks are rocks that originate near the Earth's surface as a result of chemical precipitation from water or cementation of loose fragments (called sediment). Clastic sedimentary rocks are formed up of pre-existing rock fragments (Clasts). Erosion, weathering, dissolution, precipitation, and lithification are the most major geological processes that lead to the formation of sedimentary rocks. Weathering loosens rock fragments, which are then moved to a basin or depression where sediment is trapped. Sedimentary rock is formed when sediment is buried deeply and crushed and cemented [10].

The aim of this study is to investigate the radionuclides and radon levels as well as compare radon levels recorded with a CR-39 detector to radon levels emitted from sedimentary rock samples obtained in Um-Bogma locality Sinai, Egypt.

Gamma spectra have been measured using P type High purity germanium detector (HPGe). The Solid State Nuclear Track Detector (SSNTD) was used to determine the radon concentration.

The present paper is arranged as follows: in Sect. 2, the experimental procedures as sample preparation and sample concentration measurements by Solid State Nuclear Track Detector (SSNTD) CR-39 we demonstrate. Section 3 presents the experimental data with the results obtained and the discussion. Section 4 contains the final conclusions which is followed by acknowledgement, the author contribution, the availability of data and material, conflicts of interest, ethical approval, and references.

2 Methodology

2.1 Site descriptions

The studied samples were from the north-western portion of Um Bogma, in south-western Sinai as shown in Fig. 1a: Geologic map of the studied area [11] The Um Bogma neighbourhood is situated in southern Sinai, to the east of the town of Abu Zeneima, on the eastern shore of the Gulf of Suez. According to Fig. 1, the region is roughly 700 km in size and is limited by latitudes 28° 50′ and 29° 05′ N and longitudes 33° 10′ and 33° 32′ E. b: Southwest Sinai: Lithostratigraphic section of Precambrian and Paleozoic rocks [12]. Due to its status as a major source of raw materials needed by numerous industries, the study region is significant. The crust stratigraphic in which uranium bearing

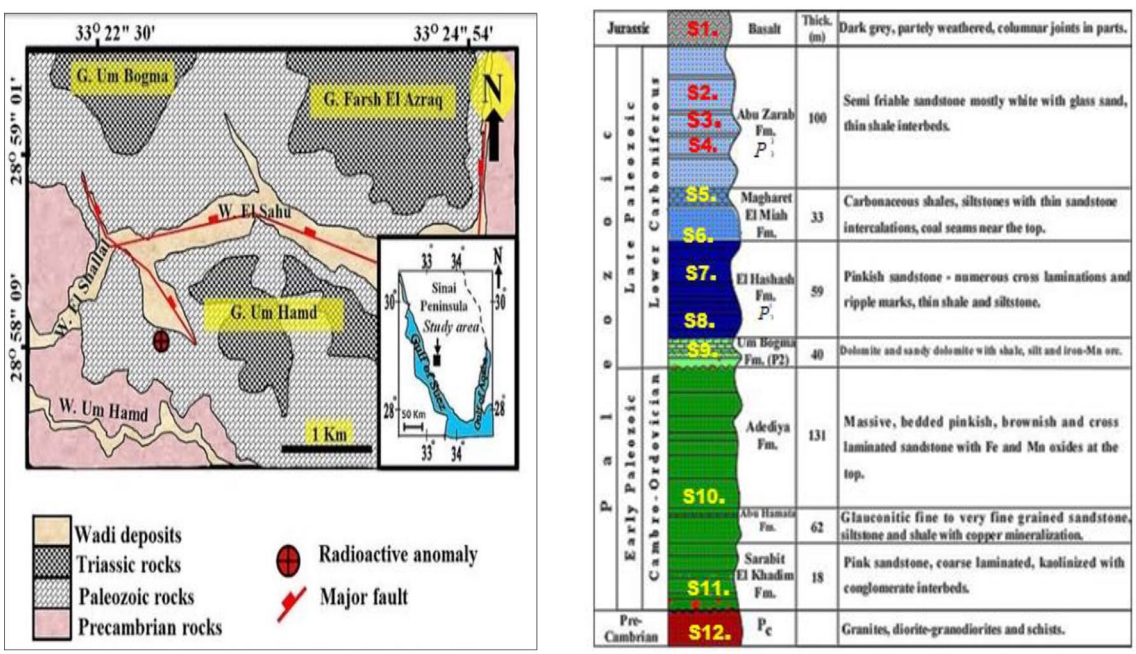

Fig. 1 **a** Geologic map of the studied area and **b** Southwest Sinai: Lithostratigraphic segment of Precambrian and Paleozoic rocks (following El Aga)

sediments are predominantly restricted and related with these formation sediments is considered in the upper Earth [13]. Industrial zones, tourism activities, mining, settlements, and land reclamation are all key development projects in South Western Sinai. The Um Bogma area is regarded as a key strategic location for some elemental production (U, Mn, Fe and Cu). The above mentioned minerals are of great benefits and very well known in different industrial domains [12].

2.2 Sample characteristics

The studied sample profile process in this component presented the formation of the lateritic profile segment and the shale containing gibbsite. When this rock unit is lateritized and karstified, it becomes extremely radioactive. Additionally karstified and lateritized, the Middle Marly Dolostone-Siltstone Member is composed of gibbsite-bearing siltstone and marl with siltstone. It is 6 to 8 m thick and only slightly radioactive. The Upper Dolostone Member, which is bedded dolostone with thin shale, is irregularly covering the karstified and lateritized soil profile [12], sample feature is listed in Table 1.

2.3 Sample preparation

Twelve sedimentary rock samples were gathered from the study region using a random sampling method. The samples were then packaged, labelled, and delivered to the lab. Each sample was dried in the open air in a dry location, mechanically crushed, and sieved through a 2 mm mesh sieve before being sealed in 100-ml polyethylene Marinelli beakers and stored to achieve secular equilibrium (preventing the escape of ^{222}Rn and ^{220}Rn) [14].

2.4 HP-Ge detector and γ-ray spectrometry:

The samples were analysed non-destructively, using a HPGe detector. The detector has a relative efficiency of approximately 40% of the 3″ × 3″ Ge (Li) crystal efficiency, with a resolution of 1.9 keV and a peak/Compton ratio of 69.9:1 at the 1332 keV gamma-ray transition of ^{60}Co. To eliminate the background radiation, a lead shield is provided with 4 mm thickness of Pb, and supported by 1 mm Cd and 1 mm Cu shield is used. Calibration of used HPGe gamma spectrometer was achieved using both ^{226}Ra point source and potassium chloride standard solutions in the same geometry as the samples. The gamma energies used for activity calculations are 352.9 keV (^{214}Pb), 609.3 keV, 1120.3 keV and 1764.5 keV (^{214}Bi) for ^{226}Ra (^{238}U) series, 338.4 keV, 911.1 keV and 968.9 keV (^{228}Ac) for ^{232}Th series, 1460.7 keV for ^{40}K, [14]. A set of IAEA (International Atomic Energy Agency) certified reference materials (IAEA-326, IAEA-375, IAEA-RGU, IAEA-CU-2008 and IAEA-152) are used for method of verification. A period of 80,000 s is adjusted for each sample and Genie 2000 software is used for gamma spectrum peak area analysis.

The following equation is used to calculate the specific activity (C) in units of Bq kg^{-1} in the current study [14]:

Table 1 Descriptions of samples

Sample code	Characterization
S1	Siltstone, grey with sulphor patches and thin fine and white sandstone laminae separating the siltstone from the overlying highly ferruginated sandstone (represents the base of El Hashash Fm.), 0.5 m
S2	Highly ferruginous sandstone, hematite with black patches of goethite, fine grained, represents the base of El Hashash Fm., 2 m, photo 140
S3	Very fine grained sandstone, thinly laminated, vary in colour, pale yellow, brown, violet with brown patches, represents the middle part of El Hashash Fm. 15 m above the previously mentioned bed, photo 139
S4	Fine pebbles of siltstone and shale represent the crashed materials
S5	Calcareous sandstone, reddish brown, directly overlying the previous fine conglomerate, it is graded upward to sandy dolomite and represents the base of middle member of Um Bogma Formation
S6	Sandydolostone, grey to light brown with turquoise patches of Cu mineralization, hard to very hard, compact; it shows gypsum laminae (2 cm) below and over the beds, photo 136 for gypsum
S7	Black shale at the center of the Quarry, fissile with gypsum interlaminae and high in organic matter contents, 0.5 m, photo 135, it needs mineral separation
S8	Sandy dolostone, light grey with brown patches, green and blue copper mineralizations, with joint fractures filled with gypsum, medium hard to hard, overlying sample No.11 (75 cm), photo 134, for green copper, it needs mineral separation
S9	Siltstone, compact, black, brown with gypsum veinlets, it is overlying the previous bed, 1.0 m
S10	Sandydolostone, dark grey to black with green copper at the surface, gypsum flakes at the joints
S11	Dolostone, bouldery, embedded in claystone and marl with gypsum at the joints and contacts, photo 132
S12	Black to dark grey shale, located below the sample No.1, rich with sulphor may be due to oxidation of pre existing pyrite, vary in thickness (1–3 m), thicker at the western part, photo 138

$$C = \frac{C_n}{\varepsilon P_\gamma M_S} \quad (1)$$

where, C_n is the count rate under each photo-peak due to each radionuclide, ε is the detector efficiency for the specific γ-ray, P_γ is the intensity of the specific γ-ray, and M_S is the mass of the sample which is measured in kg in our study.

The lowest limits of detection (LLD) is determined using the following formula [14]

$$[\text{LLD}] = \frac{4.66 S_b}{\varepsilon I_\gamma} \quad (2)$$

where: S_b is the estimated standard error of the net background count rate in the spectrum of the radionuclide.

For ^{40}K, ^{238}U, and ^{232}Th, the LLD values were 8.22, 1.98, and 1.12 Bq kg^{-1}, respectively.

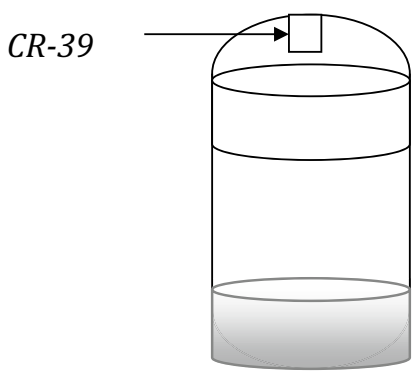

Fig. 2 CR-39 Set up in Chamber Cover

2.5 Solid state nuclear track detector (SSNTD) CR-39

SSNTD are sensitive to alpha particles in the same energy range as radon particles. The SSNTD is one of the most important tools for radon measurements [15]. (CR-39) detectors with a 1 cm × 1 cm area and a 1 mm thickness were employed. As illustrated in Fig. 2, the detectors were prepared and installed in the bottom of the chamber lid. The samples were kept for 30 days after the compartment was shut. The tracks of alpha particles from the decay of radon and its daughters that had entered the air volume of the chamber were recorded in the CR-39 during this exposure duration. The detectors were removed from the chamber cover and chemically etched at 70 °C for 6 h in a 6.25 N of NaOH solution due to radon decay, to display and expand the latent alpha tracks density was counted using the optical microscope (Fig. 3).

2.6 Radon concentration measurement

The etched traces on the detectors were manually numbered by analysing images obtained with a × 400 magnification optical microscope. A stage eyepiece was used to quantify the area of one field of vision, and the track density was measured in tracks per cm^2; the background track density was established by etching a virgin detector under the identical conditions. The background was subtracted from the measured track density.

Twenty fields of view were chosen at random on the detector surface to obtain realistic statistics of the tracks. The calibration factor of 0.18 ± 0.002 tracks cm^{-2}, acquired from a previous track detector calibration experiment (CR-39) [16], was used to compute the radon activity from the track density according to the following equation given by [17]:

Fig. 3 Distribution of activity concentrations for different radionuclides in (Bq kg^{-1})

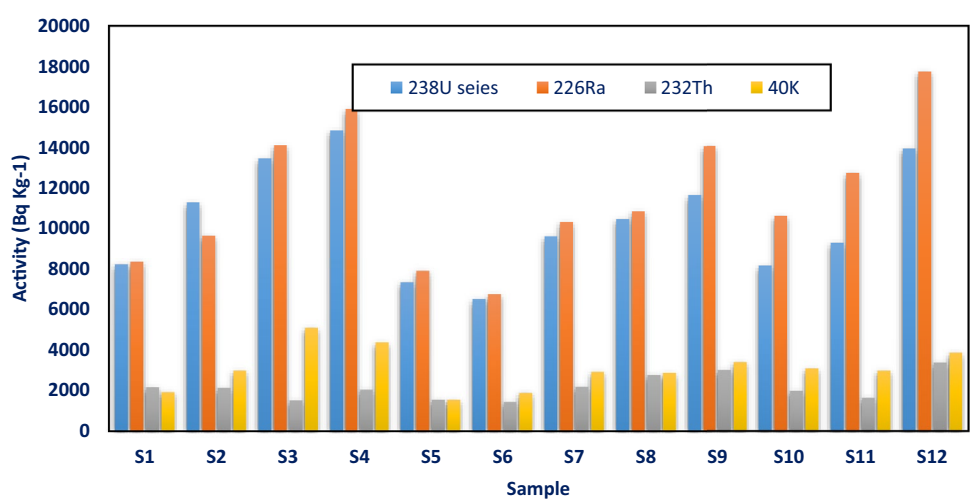

$$C_{Rn} = \frac{(N - B)}{tC_F} \quad (3)$$

where C_{Rn} is the mean ^{222}Rn concentration in Bq m^{-3}, N is the track density (Track cm^{-2}), B is the background track density (Track cm^{-2}), C_F is the calibration factor in cm^{-2} day^{-1} per Bq m^{-3}, and t is the exposure duration (in hours).

Empirical formulas with the following structure were used to calculate the amount of ^{222}Rn emitted from samples as a result of ^{226}Ra decay [18]:

$$A_R = C_R \cdot \rho \cdot A_{Ra} \quad (4)$$

where: A_R is concentration of radon gas emanated from collected sample (Bq m^{-3}). C_R is the emission constant of ^{222}Rn from collected sample, which is equal to 0.1. ρ is the sample bulk density in (kg m^{-3}) in our study. A_{Ra} is ^{226}Ra activity concentrations present in sample (Bq kg^{-1}).

3 Results and discussion

3.1 Gamma- ray counting

Table 2 presents the activities concentration of ^{238}U, ^{226}Ra, ^{232}Th and ^{40}K. One can observe in Fig. 2 that Talet Seleim Region recorded the maximum radiation level.

The specific activity in Bq kg^{-1} for ^{238}U ranged from 8182.56 to 14,853.17 with an average 10,410.83, ^{226}Ra from 6711.19 to 15,332.24 with an average 10,300.29, ^{232}Th ranged from 1436.78 to 3349.92 with an average 2141.60. Finally, the obtained results for ^{40}K ranged from 1547.22 to 5088.93 with an average 3066.40.

The physical features of the rocks and the following geochemical processes are the key variables influencing uranium distribution in the Um Bogma Formation in southwest Sinai. The diagenetic processes are of great importance in improving the physical properties of the carbonate rocks for minerals deposition.

One of the isochemical processes that result in stylolites and secondary porosity is dissolution. Mn–Fe oxides, which play a role in uranium distribution, occupied the majority of the channel porosity. Some routes for uranium solutions were formed as a result of the compaction. As well as the cementation of clastic rocks beneath carbonate rocks, creates a barrier that traps uranium solutions, resulting in peneconcordant uranium mineralization.

Figure 4 shows the activity relationship between ^{226}Ra and ^{238}U; a medium correlation $R^2 = 0.80$ (R^2 correlation is automatically calculated by Excel chart), has been found between ^{238}U and its daughter ^{226}Ra, with a positive correlation between ^{238}U and ^{226}Ra due to recent migration of uranium.

Figure 5 depicts the ^{40}K–^{232}Th relationship; bad correlation $R^2 = 0.04$ between the two has been discovered.

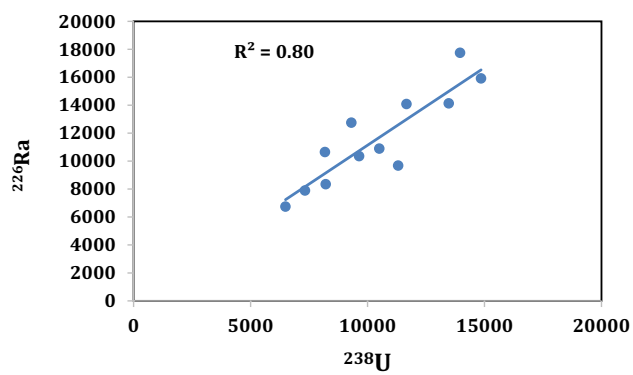

Fig. 4 Activity concentrations (Bq kg^{-1}) of ^{226}Ra vs ^{238}U for different samples

Table 2 Distribution of activity concentrations for different radionuclides in (Bq kg^{-1})

Sample	^{238}U series	^{226}Ra subseries					^{232}Th	^{40}K
	^{234}Pa	^{226}Ra	^{214}Pb	^{214}Bi	Average			
S1	8213.48 ± 51.22	6711.19 ± 92.03	8758.77 ± 73.20	9552.17 ± 89.35	8340.71 ± 102.34		2156.04 ± 81.59	1917.48 ± 58. 02
S2	11,309.44 ± 31.25	9713.88 ± 68.05	10,779.55 ± 89.12	8523.64 ± 94.10	164.60 ± 1.90		2120.52 ± 66.05	2988.89 ± 14.65
S3	13,471.33 ± 63.41	12,722.32 ± 85.91	14,149.00 ± 101.33	15,492.20 ± 71.19	1007.20 ± 6.10		1515.52 ± 69.78	5088.93 ± 42.53
S4	14,853.17 ± 27.91	14,403.45 ± 96.22	15,887.83 ± 99.12	17,427.45 ± 107.63	206.10 ± 2.50		2042.31 ± 31.02	4364.68 ± 41.93
S5	7326.59 ± 66.09	7101.72 ± 70.18	7995.96 ± 27.18	8561.23 ± 82.45	120.10 ± 1.80		1556.90 ± 51.89	1547.22 ± 12.42
S6	6493.93 ± 12.58	6220.53 ± 45.97	6798.57 ± 14.51	7196.23 ± 78.30	386.70 ± 3.80		1436.78 ± 26.75	1885.01 ± 34.52
S7	9640.89 ± 101.02	8919.77 ± 55.14	10,621.57 ± 79.32	11,511.50 ± 109.02	144.02 ± 2.10		2181.25 ± 14.95	2914.96 ± 41.68
S8	10,504.98 ± 86.50	10,068.54 ± 71.39	10,995.53 ± 94.75	11,590.45 ± 88.62	15.30 ± 0.40		2757.56 ± 76.34	2860.38 ± 16.22
S9	11,665.58 ± 106.07	12,183.62 ± 100.09	14,544.71 ± 49.62	15,509.39 ± 87.12	314.90 ± 3.30		2989.30 ± 32.71	3374.96 ± 45.81
S10	8182.56 ± 92.11	9281.39 ± 32.11	11,074.79 ± 93.16	11,563.97 ± 79.65	112.80 ± 1.90		1963.81 ± 21.35	3063.16 ± 11.86
S11	9309.95 ± 60.87	10,944.85 ± 69.01	13,088.55 ± 112.61	14,208.40 ± 62.39	230.30 ± 3.70		1629.24 ± 21.06	2958.07 ± 12.77
S12	13,958.02 ± 102.03	15,332.24 ± 113.69	18,390.68 ± 76.14	19,510.35 ± 31.08	1506.60 ± 9.20		3349.92 ± 23.09	3833.06 ± 29.17
Average	10,410.83 ± 54.23	10,300.29 ± 72.43	11,923.79 ± 22.96	12,553.91 ± 44.08	8340.71 ± 93.68		2141.60 ± 41.76	3066.40 ± 94.82

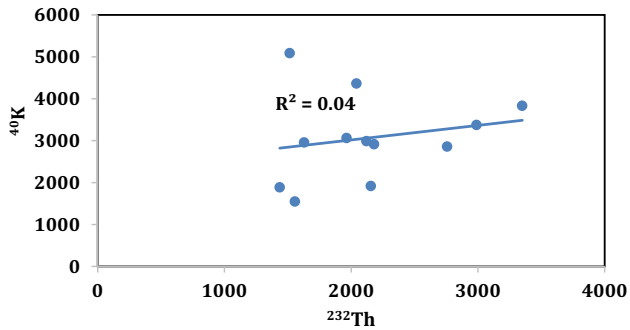

Fig. 5 Activity concentrations (Bq kg^{-1}) of ^{40} K vs ^{232}Th for different samples

Thorium is now estimated to be three times more plentiful than uranium [19].

3.2 Radon concentration

Radon concentrations from CR-39 recorded tracks were calculated using Eq. 3, and compared with expected radon emission by using Eq. 4 according to radium activity measured by gamma counting of different studied samples as presented in Table 3.

By confining the sample in a closed chamber and observing the rise in radon concentration, the amount of radon activity released into the air per unit time from the samples with different radium concentrations in its structure matrix has been calculated using equation Loss of measured radon that has been listed in Table 2, as shown in the demonstrated values the maximum loss is corresponding to the highest radium activity. The inclusion of thin layers containing Ra has been demonstrated to boost Rn emission from grains. To create a nonuniform Ra distribution, a multiple-recoil technique is proposed [20]. As a result, only radon that has been recoiled and is still in the water or air phase for free diffusion is deemed to have been emitted [21]. Recoiled radon that has passed through the water and air phases and is now lodged in a neighbouring solid is referred to as embedded radon [22].

Due to their extremely low diffusion coefficients in solids, radon atoms contained within solid grains are unlikely to become available for emission to the environment. Nevertheless, if they are found in the voids between grains, they may spread to the top. Consequently, radon emissions from a residue repository are caused by the following set of processes to the atmosphere [23]:

(a) Emanation: Radon atoms produced by the disintegration of radium escape from the grains into the interstitial space between the grains, primarily due to recoil.
(b) Transport: The emitted radon atoms migrate through the residue or soil profile and reach the ground surface as a result of diffusion and advective flow.
(c) Exhalation, which involves the release of radon atoms into the atmosphere after they have travelled to the ground surface.

Due to the various aforementioned causes, there has been a large percentage of loss for measured radon compared to expected emitted radon corresponding to radium activities in different studied samples.

Figure 6 displays the correlation of loss of radon present and sample density. As shown in figure, good correlation $R^2 = 0.98$ has been found. This explains the sample structure effect on the distribution of radium on the grain surface [24].

For ^{238}U, ^{232}Th series, and ^{40}K, the global median concentrations are 35 Bq kg^{-1}, 30 Bq kg^{-1} and 400 Bq kg^{-1}, respectively [19]. As a result, the mean activity of these

Table 3 Experimental and Calculated of Radon Concentration (Bq/L)

Sample	RnC_{exp} (Bq L^{-1})	Mass (g)	ρ	^{226}Ra (Bq kg^{-1})	^{226}Ra (Bq L^{-1})	RnC_{cal} (Bq L^{-1})	Loss%
S1	41,175.45	264.6	1.32	6711	8.88E+06	67,111.9	38.65
S2	45,428.04	274.4	1.37	9714	1.33E+07	97,138.8	53.23
S3	50,323.68	241.2	1.21	12,722	1.53E+07	127,223.2	60.44
S4	53,884.44	261.8	1.31	14,403	1.89E+07	144,034.5	62.59
S5	56,735.64	263.5	1.32	7102	9.36E+06	71,017.2	20.11
S6	53,822.88	224.4	1.12	6221	6.98E+06	62,205.3	13.48
S7	46,400.04	232.9	1.16	8920	1.04E+07	89,197.7	47.98
S8	50,255.64	249.6	1.25	10,069	1.26E+07	100,685.4	50.09
S9	53,790.8	239.4	1.2	12,184	1.46E+07	121,836.2	55.85
S10	45,428.04	265.2	1.33	9281	1.23E+07	92,813.9	51.05
S11	50,288.04	245.1	1.23	10,945	1.34E+07	109,448.5	54.05
S12	62,345.81	257.6	1.29	12,926	16,134.71	138,435.90	54.96

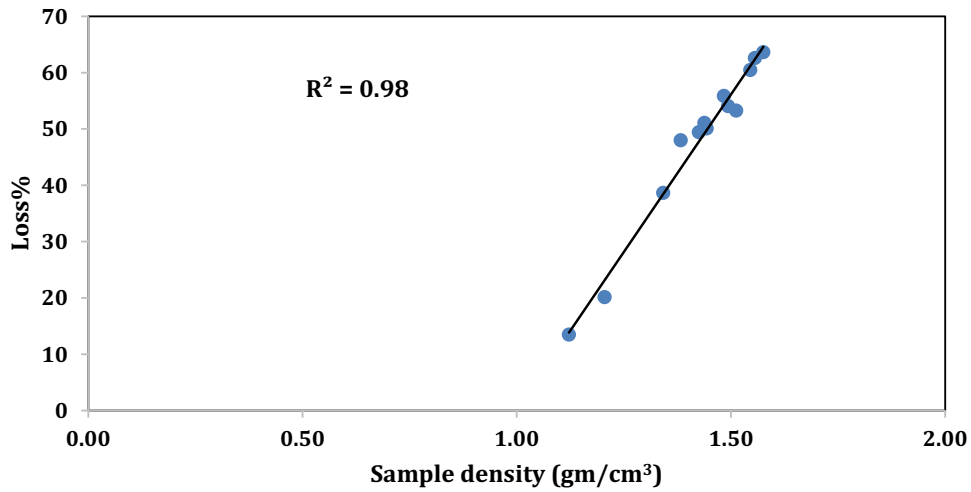

Fig. 6 Correlation between Loss percent of Radon and sample density

radionuclides in the examined samples are higher than the global median range for ^{238}U.

Levels of radioactivity concentration of the selected samples from studied area show anomaly and above permissible level which in coincidence with previous work [12].

As shown in the above displayed results, anomalous radioactive levels for ^{238}U and ^{226}Ra have been detected in areas with habitation, this explains the loss of uranium to the ground water that was previously observed in this area [25].

Correlation between parent/daughter or any other progeny pairs can be used to gauge the persistence of the original proportionality between the ^{238}U decay series.

4 Conclusions

Our study was to look at the amount of radionuclides in the Um-Bogma area. This was accomplished by employing gamma counting and SSNTD to measure radioactive activity and radon concentration as well as predicted radon.

The average activity concentration of radionuclides in different samples was displayed, suggesting that the ^{238}U level in all of the soils studied was significant. The major findings are shortened as under.

1. The specific activity in Bq kg^{-1} for ^{238}U ranged from 8182.56 to 14,853.17 with an average 10,410.83, ^{226}Ra from 6711.19 to 15,332.24 with an average 10,300.29, ^{232}Th ranged from 1436.78 to 3349.92 with an average 2141.60. Finally, the obtained results for ^{40}K ranged from 1547.22 to 5088.93 with an average 3066.40.
2. The physical features of the rocks and the following geochemical processes are the key variables influencing uranium distribution in the Um Bogma Formation in southwest Sinai. The diagenetic processes are of great importance in improving the physical properties of the carbonate rocks for minerals deposition.
3. The cementation of clastic rocks beneath carbonate rocks, creates a barrier that traps uranium solutions, resulting in peneconcordant uranium mineralization.
4. In the ^{40}K–^{232}Th relationship; bad correlation $R^2 = 0.04$ between the two has been discovered. Thorium is now estimated to be three times more plentiful than uranium
5. In the correlation of loss of radon present and sample density; good correlation $R^2 = 0.98$ has been found. This explains the sample structure effect on the distribution of radium on the grain surface.
6. For ^{238}U, ^{232}Th series, and ^{40}K, the global median concentrations are 35 Bq kg^{-1}, 30 Bq kg^{-1} and 400 Bq kg^{-1}, respectively [20]. As a result, the mean activity of these radionuclides in the examined samples are higher than the global median range for ^{238}U.

Our future direction is order to determine the exposure limits for local residents and visitors, as well as to understand the thermal effects of radiation levels, it will be necessary to gradually include areas with residential activity in the measurement of the distribution of radioactive nuclei across the entire Sinai region.

Acknowledgements This work is measured in nuclear physics lab at Physics Department, Faculty of Women for Arts, Science and Education, Ain Shams University, Egypt. The authors, therefore, gratefully acknowledge all members of the lab.

Author contributions Author contributions conceptualization: DG; methodology: LKB; formal analysis and investigation, writing-review and editing: DG and LKB. All authors read and approved the final manuscript.

Funding Open access funding provided by The Science, Technology & Innovation Funding Authority (STDF) in cooperation with The Egyptian Knowledge Bank (EKB). No funds, grants or other support was received.

Data availability The authors declare that all data generated or analysed during this study are included in this published article.

Declarations

Conflict of interest The authors have no relevant financial or non-financial interests to disclose.

Ethical approval This article does not contain any studies with human participants or animals performed by any of the authors.

Open Access This article is licensed under a Creative Commons Attribution 4.0 International License, which permits use, sharing, adaptation, distribution and reproduction in any medium or format, as long as you give appropriate credit to the original author(s) and the source, provide a link to the Creative Commons licence, and indicate if changes were made. The images or other third party material in this article are included in the article's Creative Commons licence, unless indicated otherwise in a credit line to the material. If material is not included in the article's Creative Commons licence and your intended use is not permitted by statutory regulation or exceeds the permitted use, you will need to obtain permission directly from the copyright holder. To view a copy of this licence, visit http://creativecommons.org/licenses/by/4.0/.

References

1. Ojovan MI, Lee WE (2014) An introduction to nuclear waste immobilisation. Elsevier Ltd, Amsterdam, pp 31–39
2. Missimer TM, Teaf C, Maliva RG, Danley-Thomson A, Covert D, Hegy M (2019) Natural radiation in the rocks, soils, and groundwater of southern Florida with a discussion on potential health impacts. Int J Environ Res Public Health 16:1793–1814
3. El Aassy IE, El Feky MG, El Kasaby MA, Ibrahim EM, Sewefi S, Attia RM (2019) Behavior of radionuclides during acidic leaching processes of different rock materials, allouga locality, Southwestern Sinai, Egypt. Int J Sci Eng Res 8:1135–1147
4. IAEA, International Atomic Energy Agency Vienna (2013) Radiation Protection and Management of Norm Residues in the Phosphate Industry, Safety reports series no. 78
5. Al-Jarallah MI, Fazal-ur-Rehman, Musazay MS, Aksoy A (2005) Correlation between radon exhalation and radium content in granite construction material in Saudi Arabia. Radiat Meas 40:625–629
6. Kölbel L, Kölbel T, Maier U, Sauter M, Schäfer T, Wiegand B (2020) Water–rock interactions in the Bruchsal geothermal system by U-Th series radionuclides. Geothermal Energy 8(1):1–33
7. El Aref M, El-Rahman A, Zoheir B, Surour A, Helmy HM, Abdelnasser A, Ahmed AH, El-Ahmadi Ibrahim M (2020) Mineral resources in Egypt (I): metallic ores, the geology of Egypt. Springer, Cham, pp 521–587
8. Mogro-Campero A, Fleischer RL, Juid S (1977) Conversion: a hydrothesis for long-distance migration of radon within the earth. Earth Planet Sci Lett 54:321–325
9. Somogyi G, Hafez A, Hunyadi I, Toth-Szilagyi M (1986) Measurement of exhalation and diffusion parameters of radon in solids by plastic track detectors. Nucl Tracks Radiat Meas 12:701–704
10. Johnson C, Affolter MD, Inkenbrandt P, Mosher C (2017) An introduction to geology Salt Lake Community college
11. Shaaban MN, Holail HM, Sedeik KN, Rashed MA (2005) Multiple dolomitization events of the lower carboniferous Um Bogma formation, west central Sinai. Egypt Carbon Evaporites 20:107–115
12. El Aassy I, El Galy M, Nada A, El Feky M, Abd El Maksoud T, Talaat S, Ibrahim E (2011) Effect of alteration processes on the distribution of radionuclides in uraniferous sedimentary rocks and their environmental impact, southwestern Sinai, Egypt. J Radioanal Nucl Chem 289(1):173–184
13. Gad A, Al-Mur BA, Alsiary WA, Abd El Bakey SM (2022) Optimization of carboniferous Egyptian kaolin treatment for pharmaceutical applications. Sustainability 14(4):2388
14. Nada A, Aly HAS (2014) The effect of uranium migration on radionuclide distributions for soil samples at the El-Gor area, Sinai, Egypt. Appl Radiat Isotopes 84:79–86
15. Mansy M, Sharaf MA, Eissa HM, El-Kamees SU, Abo-Elmagd M (2006) Theoretical calculation of SSNTD response for radon measurements and optimum diffusion chambers dimensions. Radiat Meas 41(2):222–228
16. Janik M, Hasan MM, Bossew P, Kavasi N (2021) Effects of storage time and pre-etching treatment of CR-39 detectors on their response to alpha radiation exposure. Int J Environ Res Public Health 18(16):8346
17. Khan AJ, Varshney AK, Parsed R, Tyagi RK, Ramachandran TV (1990) Calibration of (CR-39) plastic track detector for the measurement of radon and its daughters in dwellings. Nucl Tracks Radiat Measure 17:497–502
18. Adel SM, Hegazy TM, Abd El Maksoud TM, Diab HM (2022) Analytical study of radionuclide and radon concentrations in rock samples collected from Um-Bogma and its radiological hazard impact. Arab J Nucl Sci Appl 55(2):1–8
19. Hynes WM (2013) CRC handbook of chemistry & physics. 93 third Edition
20. UNSCEAR (2000) Sources and effects of ionizing radiation. United Nations Scientific Committee on the Effect of Atomic Radiation, New York
21. Semkow TM, Parekh PP (1990) The role of radium distribution and porosity in radon emanation from solids. Geophys Res Lett 17(6):837–840
22. Sun H, Furbish DJ (1995) Moisture content effect on radon emanation in porous media. J Contamin Hydrol 18(3):239–255
23. Sakoda A, Ishimori Y (2017) Mechanisms and modeling approaches of radon emanation for natural materials. Jpn J Health Phys 52(4):296–306
24. Moed BA, Nazaroff WW, Sextro RG (1988) "Soil as a source of indoor radon: Generation, migration and entry. In: Nazaroff WW, Nero AV Jr (eds) Radon and its Decay Products in Indoor Air. Wiley, New York, pp 57–112
25. Ramadan RS, Dawood YH, Yehia MM, Gad A (2022) Environmental and health impact of current uranium mining activities in southwestern Sinai, Egypt. Environ Earth Sci 81:213

Publisher's Note Springer Nature remains neutral with regard to jurisdictional claims in published maps and institutional affiliations.